Fermi National Accelerator Laboratory

FERMILAB-Pub-75/48-EXP
7100.096

(Submitted to Phys. Rev. Letters)

MEASUREMENT OF ELASTIC SCATTERING OF HADRONS ON PROTONS FROM 50 TO 175 GeV/c

Fermilab Single Arm Spectrometer Group

July 1975

Operated by Universities Research Association Inc. under contract with the Energy Research and Development Administration

FERMILAB-Pub-75/48-EXP
ANL-HEP-PR-75-26
COO-3130PB-215

Measurement of Elastic Scattering of Hadrons on Protons from 50 to 175 GeV/c*

Fermilab Single Arm Spectrometer Group†

July, 1975

Abstract

Differential cross sections have been measured at Fermilab with a focusing spectrometer for $\pi^{\pm}p$, $K^{\pm}p$, and $p^{\pm}p$ elastic scattering at 50, 70, 100, 140, and 175 GeV/c incident momentum over the $|t|$ range 0.03 to 0.8 GeV^2. The results are smooth in t and are parameterized by quadratic exponential fits.

*Work supported in part by the U.S. Energy Research and Development Administration, the National Science Foundation, and INFN (Italy).

†D. S. Ayres, R. Diebold, G. J. Maclay, Argonne National Laboratory; D. Cutts, R. E. Lanou, L. J. Levinson, and J. T. Massimo, Brown University; J. Litt, CERN and Daresbury Laboratory; R. Meunier, CERN and CEN Saclay; B. Gittelman, E. Loh, and M. Sogard, Cornell University; A. E. Brenner, J. E. Elias, and G. Mikenberg, Fermi National Accelerator Laboratory; L. Guerriero, P. Lavopa, G. Maggi, C. DeMarzo, F. Posa, G. Selvaggi, P. Spinelli, F. Waldner, E. F. Anelli, Bari University, INFN-Bari, Italy; D. S. Barton, J. Butler, J. Fines, J. I. Friedman, H. W. Kendall, B. Nelson, L. Rosenson and R. Verdier, Massachusetts Institute of Technology; B. Gottschalk, Northeastern University; R. L. Anderson, D. Gustavson, K. Rich, D. M. Ritson, and G. A. Weitsch, Stanford Linear Accelerator Center.

This paper describes measurements of $\pi^{\pm}p$, $K^{\pm}p$ and $p^{\pm}p$ elastic scattering in the energy region recently made accessible at the Fermi National Accelerator Laboratory. The reactions were studied for momentum transfers $|t|$ from 0.03 to 0.8 GeV^2 and incident momenta of 50, 70, 100, 140, and 175 GeV/c, with about 10^6 events total at each energy.

The experiment was carried out in the Meson Laboratory at Fermilab using the single arm spectrometer in the M6E beam line. Detailed descriptions of the spectrometer and beam will be published separately and only a brief description is given here.

M6E is a high-energy, high-resolution unseparated secondary particle beam at 2.8 mrad to the external proton beam. Each of its three stages has point-to-parallel-to-point optics with bending magnets located in the parallel regions. In the first stage collimators define the solid angle and momentum acceptances to maximum values of 1.75 μster and 1.2% respectively. The second stage serves to clean up the beam and removes almost all of the halo. In the third stage the dispersed beam is momentum recombined and focused to a small spot at the hydrogen target, typically 6 mm by 3 mm. Five scintillation counter hodoscopes, a threshold Cerenkov counter, a differential Cerenkov counter, and a DISC counter[1] in the third stage provide full tagging of the incident beam momentum, trajectory, and particle type. This allows the simultaneous measurement of cross sections for incident pions, kaons, and protons. Beam fluxes of typically 3×10^6/burst were used in this experiment.

The spectrometer also has point-to-parallel-to-point optics. Scintillation counters and/or proportional wire chamber cuts defined the spectrometer acceptance regions of typically 5 μster, ±1.5 mrad scattering angle, and ±2% Δp/p. Ten proportional wire chambers, a hodoscope, three threshold Cerenkov counters, and a differential Cerenkov counter[2] were used for full tagging of the trajectory and particle type. For straight-through beam tracks, the rms differences between the beam and spectrometer measurements were typically ±0.07% in momentum and ±0.13 mrad in scattering angle.

Three bending magnets located just upstream of the hydrogen target were used to vary the momentum transfer by pitching the incident beam in the vertical plane to a maximum angle of ±25 mrad. In order to maintain alignment with the beam as the angle is varied, the final beam line components, counters, hodoscopes, and hydrogen target could all be remotely adjusted. The target cells, which were one-inch diameter Mylar tubes, 10 and 20 inches long, only required a pitch adjustment to track the scattering angle variations, as the beam crossed the spectrometer axis at the midpoint of the targets. The field of the angle-varying magnets, as well as the beam and spectrometer momentum values, were continuously monitored with Rawson probes located in three-foot long monitor magnets connected in series with the appropriate bending magnets. Measurements were made with both positive and negative deflection angles to average out any systematic errors caused by small misalignments. The t values were determined directly in terms of the magnetic field calibration to a precision of about 0.3%.

Scattered events mixed with an unbiased sample of beam events were used as triggers. The sample of beam events permitted determinations of beam line detector efficiences, the beam phase-space distribution, and the effects of any fiducial cuts on incoming particle fluxes. A PDP-11/45 computer operating under the SPEX multitask system[3] was used to analyze data online for monitoring purposes and to record the data onto magnetic tape for subsequent analysis. Up to 200 events per beam burst could be recorded.

The missing-mass squared (M_x^2), t, and particle type were determined for each event. Figure 1 is a typical M_x^2 distribution showing the separation of the elastic peak from inelastic background. The resolution function was known to be symmetric from straight-through runs and a fit was made to the M_x^2 distribution to determine the inelastic contamination under the elastic peak. Typically, this background was 3% and was known to about 1%.

Under most running conditions the contamination through misidentification of the incoming particle type was small and well determined. Muon and electron contaminations of the incoming beam were measured independently and were each ~1%.

The total detection efficiency of the spectrometer system including the wire chambers was typically 95% and the absolute efficiency was known to about ±1%. The presence of two simultaneous incoming particles was virtually eliminated by requiring only one particle in the beam line hodoscopes.

Corrections for decay-in-flight and attenuation in the target were calculated, and also measured from the transmission of the straight-through, unscattered beam into the spectrometer. Small corrections were applied for multiple Coulomb scattering, double nuclear scattering, and Coulomb interference effects. Radiative corrections were made according to the prescription of Sogard,[4] and were a few percent for pions and considerably less for kaons and protons.

The spectrometer solid angle was calculated from the known magnetic and geometric properties of the spectrometer and verified by direct measurement at each momentum. An overall check of the normalization was made by comparing our pp results with the data of Bartenev et al.[5] at $|t| = 0.09$ GeV^2. Agreement was found within 3%.

The pion and proton events were restricted by cuts to a well-understood region of the spectrometer to give absolute cross sections. The low-rate particles, $K^{\pm}$ and $\bar{p}$, were accepted over the entire aperture of the spectrometer and the corresponding solid angle obtained from the pion and proton fluxes.

The overall normalization uncertainty is ± 3%, independent of t. In addition, there is an uncertainty increasing from ± 1% at small t to ± 6% at 0.8 GeV^2 due to uncertainties in the inelastic contamination, the double-scattering corrections, and the determination of the scattering angle. Decay-in-flight corrections were only significant for kaons, and at 50 GeV/c (where 25% decay in the spectrometer) there is an additional 3% systematic uncertainty.

Our differential cross section data in the range $0.03 \leq |t| \leq 0.8$ GeV^2 cannot be fit with a simple exponential, but may be represented by

$$\frac{d\sigma}{dt} = A \exp (Bt + Ct^2) \quad . \tag{1}$$

This form gives a good representation of the data and a typical set of fits is shown in Fig. 2. Table I lists the parameters of these fits. Our results at 50 GeV/c are in good agreement with those from Serpukhov[6,7] at 40 and 50 GeV/c, and with the optical points derived from total cross section measurements.[8]

Table I also includes the logarithmic slope parameters defined as

$$b(|t|) = \frac{d}{dt} (\ln \frac{d\sigma}{dt}) = B - 2C|t| \quad , \tag{2}$$

evaluated at 0.2 GeV^2. Figure 3 shows that our values for b(0.2) connect smoothly to previous results[6,7] at other energies. The $\pi^{\pm}$ and K^- slopes show little energy dependence, while the K^+ and proton slopes are gradually increasing.

While the data for all reactions studied are well described by the fits to Eq. (1), other forms such as piecewise linear exponentials, as suggested by Carrigan[9] and CERN ISR data,[10] are also possible. The values of C listed in Table I indicate a decrease in the logarithmic slope $\Delta b = 2C\Delta t \approx 2$ GeV^{-2} in going from $|t| = 0.1$ to 0.5 GeV^2.

The crossover points, where particle and antiparticle have equal cross sections, were calculated from fits to Eq. (1) using data with $|t| < 0.4$ GeV^2. Our $K^{\pm}p$ and $p^{\pm}p$ data are consistent with crossover points in the range $|t| = 0.15 \pm 0.08$ GeV^2, with no obvious energy variation. This

is similar to the values of 0.19 and 0.16 GeV^2 observed previously[11] in the region 3 to 6 GeV/c for $K^{\pm}p$ and $p^{\pm}p$, respectively.

We would like to thank the many people at Fermilab who have contributed to the successful construction and operation of the Single Arm Spectrometer Facility. We would also like to express appreciation to our technical support personnel for their invaluable assistance in the instrumentation of the facility.

References

1. M. Benot, J. Litt and R. Meunier, Nucl. Instr. and Meth. 105, 431 (1972).
2. Single Arm Spectrometer Facility Group, "Search for Heavy Mass Particles and Antideuteron Flux Produced by 300 GeV Protons on Beryllium," NAL-73/83-EXP 7100.096, 1973 (unpublished).
3. L. J. Levinson et al., Bull. Am. Phys. Soc. 20, 593 (1975).
4. M. Sogard, Phys. Rev. D9, 1486 (1974).
5. V. Bartenev et al., Phys. Rev. Letters 31, 1088 (1973).
6. A. A. Derevchekov et al., Phys. Letters 48B, 367 (1974).
7. Yu. M. Antipov et al., Nucl. Phys. B57, 333 (1973); S. Nurushev, XVII Int. Conf. on High Energy Physics, London, 1974, p. I-25.
8. A. S. Carroll et al., Phys. Rev. Letters 33, 928 and 932 (1974).
9. R. A. Carrigan, Jr., Phys. Rev. Letters 24, 168 (1970).
10. U. Amaldi et al., Phys. Letters 36B, 504 (1971); G. Barbiellini et al., Phys. Letters 39B, 663 (1972).
11. I. Ambats et al., Phys. Rev. D9, 1179 (1974).

Table Caption

Table I. Results of fitting the differential cross sections to Eq. (1). A, B and C are from fits to data out to $|t| = 0.8$ GeV^2; only statistical errors were used for the data points, while the optical theorem point (Opt. Pt., Ref. 8) was included with a ±3% error to account for the uncertainty in absolute normalization. The values of the logarithmic slope at $|t| = 0.2$ GeV^2 were found from Eq. (2) using fits to data with $|t| < 0.4$ GeV^2; the errors shown include a systematic error of ±0.15 GeV^{-2} added in quadrature to the statistical errors. The total elastic cross sections were obtained by integrating fits (with A fixed to the optical point) out to $|t| = 0.8$ GeV^2; a small correction was made for contributions at larger t by assuming a constant logarithmic slope at $|t| \geq 0.8$ GeV^2.

Figure Captions

Fig. 1 Missing-mass squared distribution showing the elastic peak for $\pi^+ p$ at 70 GeV/c for $0.04 \leq |t| \leq 0.18$ GeV^2.

Fig. 2 Differential cross sections for elastic scattering at 100 GeV/c. The optical theorem point is shown at t = 0. The error bars for many points fall within the symbols. The curves are best fits to Eq. (1) with the parameters listed in Table I.

Fig. 3 Logarithmic slopes at $|t| = 0.2$ GeV^2 as a function of s, the total energy squared in the center of mass. The lines are drawn only to guide the eye. Data sources: □ = Ref. 6; ○, △ = Ref. 7; ●, ▲ = this experiment.

Table I

		Opt. Pt.	A	B	C	b(0.4)	σ_{elas}
	(GeV)	(mb/GeV^2)	(mb/GeV^2)	(GeV^{-2})	(GeV^{-4})	(GeV^{-2})	(mb)
π^+p	50	27.2	27.8 ± 0.4	8.85 ± 0.12	1.92 ± 0.18	8.07 ± 0.17	3.33 ± 0.07
	70	27.5	27.7 ± 0.5	8.98 ± 0.14	2.35 ± 0.23	8.08 ± 0.17	3.31 ± 0.08
	100	27.7	27.5 ± 0.8	8.80 ± 0.18	2.12 ± 0.23	7.92 ± 0.20	3.33 ± 0.09
	140	28.1	29.1 ± 0.6	9.11 ± 0.17	2.36 ± 0.28	8.18 ± 0.17	3.42 ± 0.08
	175	28.5	29.2 ± 0.4	9.02 ± 0.10	2.26 ± 0.15	8.16 ± 0.16	3.46 ± 0.07
π^-p	50	29.5	31.7 ± 0.4	9.74 ± 0.11	3.07 ± 0.15	8.61 ± 0.17	3.53 ± 0.07
	70	29.4	28.3 ± 0.5	8.92 ± 0.20	2.07 ± 0.47	7.97 ± 0.17	3.37 ± 0.10
	100	29.3	27.4 ± 0.5	9.04 ± 0.14	2.38 ± 0.20	8.09 ± 0.17	3.25 ± 0.07
	140	29.6	29.0 ± 0.6	9.20 ± 0.18	2.40 ± 0.29	8.17 ± 0.18	3.37 ± 0.09
	175	29.9	29.2 ± 0.8	9.66 ± 0.18	2.88 ± 0.24	8.59 ± 0.19	3.26 ± 0.08
K^+p	50	16.6	17.1 ± 0.4	6.95 ± 0.29	0.42 ± 0.59	6.94 ± 0.31	2.51 ± 0.12
	70	17.3	17.8 ± 0.4	7.65 ± 0.26	1.31 ± 0.54	7.30 ± 0.23	2.44 ± 0.10
	100	18.2	18.0 ± 0.5	7.79 ± 0.32	1.89 ± 0.54	6.98 ± 0.24	2.50 ± 0.11
	140	19.1	19.0 ± 0.7	8.50 ± 0.28	2.39 ± 0.43	7.61 ± 0.28	2.43 ± 0.09
	175	19.6	19.2 ± 0.4	8.52 ± 0.16	2.20 ± 0.28	7.63 ± 0.19	2.42 ± 0.06
K^-p	50	21.0	21.1 ± 0.7	8.73 ± 0.34	2.30 ± 0.61	8.28 ± 0.43	2.60 ± 0.11
	70	21.0	19.9 ± 0.7	8.11 ± 0.59	1.05 ± 1.63	7.52 ± 0.48	2.55 ± 0.19
	100	21.3	21.0 ± 0.7	9.16 ± 0.40	3.20 ± 0.71	7.48 ± 0.35	2.54 ± 0.12
	140	21.6	21.8 ± 0.5	9.03 ± 0.27	2.49 ± 0.58	8.03 ± 0.18	2.61 ± 0.09
	175	21.9	22.2 ± 0.7	9.46 ± 0.31	3.00 ± 0.63	8.37 ± 0.27	2.55 ± 0.09
pp	50	76.2	75.3 ± 0.7	10.28 ± 0.11	1.42 ± 0.23	9.67 ± 0.16	7.55 ± 0.14
	70	75.0	72.9 ± 1.2	10.73 ± 0.17	1.91 ± 0.30	10.03 ± 0.17	7.05 ± 0.15
	100	76.0	75.6 ± 1.8	10.95 ± 0.21	2.05 ± 0.36	10.19 ± 0.18	7.17 ± 0.17
	140	76.2	75.5 ± 1.4	11.30 ± 0.13	2.49 ± 0.20	10.37 ± 0.17	6.99 ± 0.12
	175	76.5	72.1 ± 1.5	10.95 ± 0.16	2.31 ± 0.29	10.00 ± 0.16	6.88 ± 0.14
$\bar{p}p$	50	98.3	99.5 ± 1.9	12.66 ± 0.25	3.13 ± 0.51	11.82 ± 0.31	8.22 ± 0.19
	70	94.0	88.0 ± 1.7	12.47 ± 0.38	2.43 ± 1.19	11.51 ± 0.33	7.31 ± 0.24
	100	90.3	92.0 ± 2.4	12.39 ± 0.34	3.97 ± 0.67	10.91 ± 0.36	7.90 ± 0.24
	140	88.9	88.3 ± 2.2	12.57 ± 0.40	3.60 ± 0.88	10.99 ± 0.28	7.41 ± 0.25
	175	88.4	85.4 ± 3.0	13.19 ± 0.43	4.38 ± 1.04	11.30 ± 0.28	6.87 ± 0.24

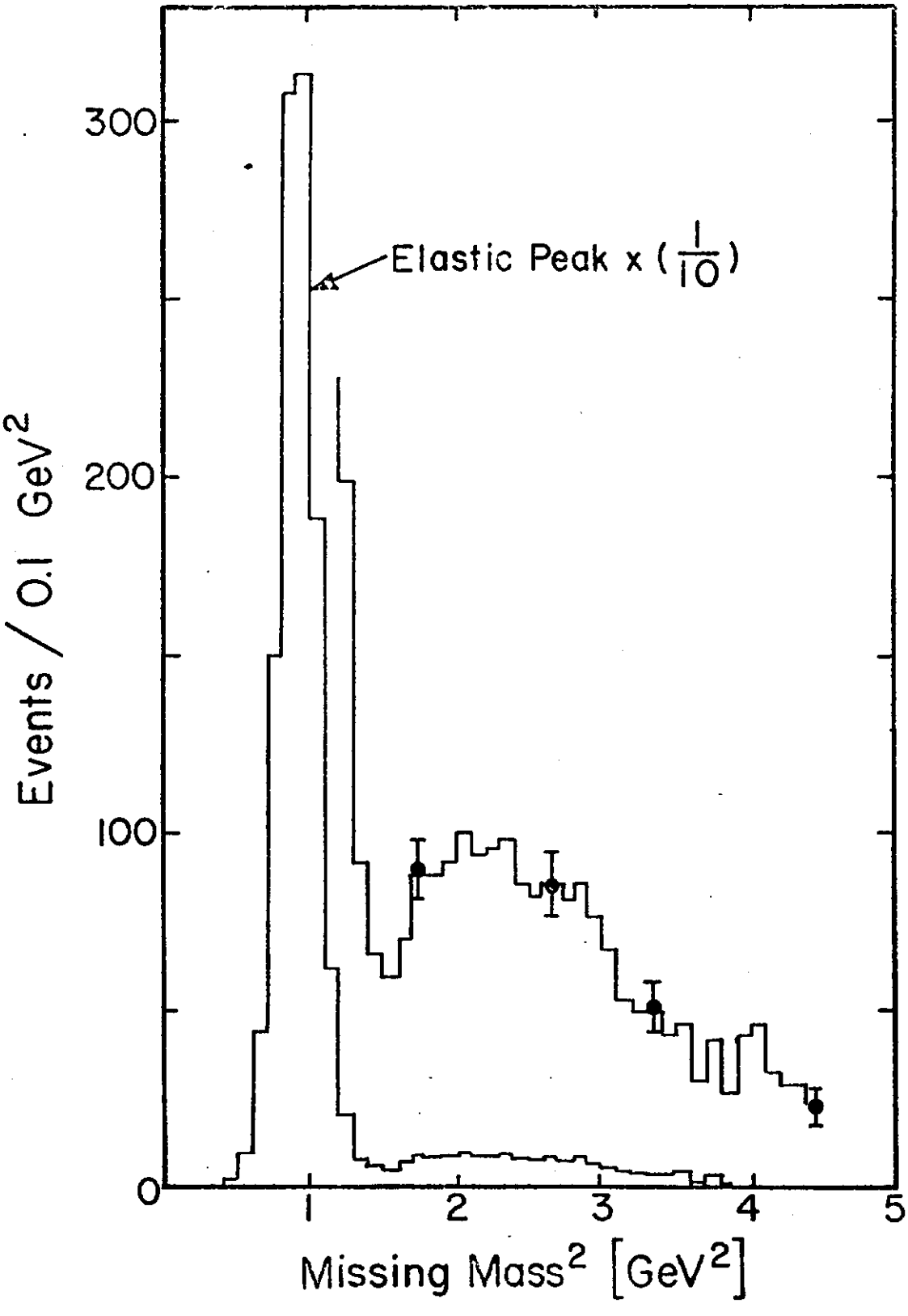
300
200
100
0
Events / 0.1 GeV²
Elastic Peak x (1/10)
1
2
3
4
5
Missing Mass² [GeV²]

Figure 1

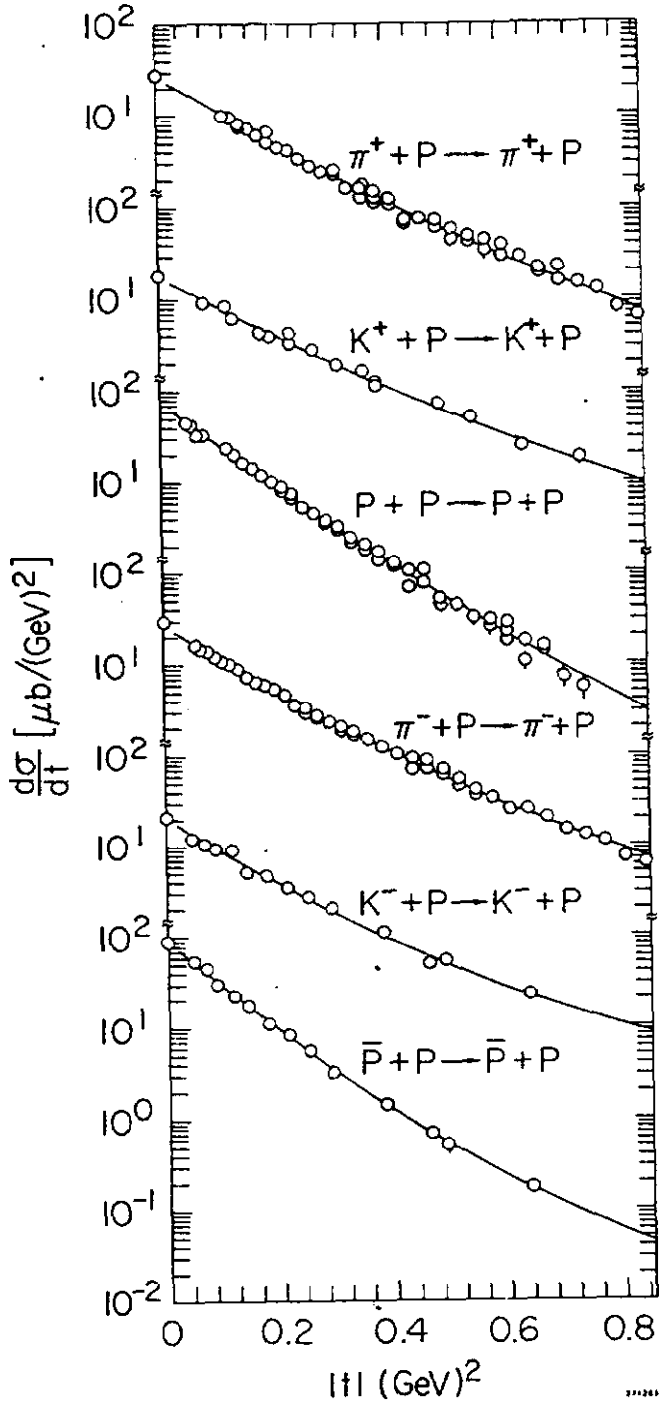
10^2
10^1
10^2
10^1
10^2
10^1
10^2
10^1
10^2
10^1
10^0
10^{-1}
10^{-2}
$\pi^+ + P \rightarrow \pi^+ + P$
$K^+ + P \rightarrow K^+ + P$
$P + P \rightarrow P + P$
$\pi^- + P \rightarrow \pi^- + P$
$K^- + P \rightarrow K^- + P$
$\bar{P} + P \rightarrow \bar{P} + P$
$\frac{d\sigma}{dt}$ [μb/(GeV)^2]
0
0.2
0.4
0.6
0.8
|t| (GeV)^2

Figure 2

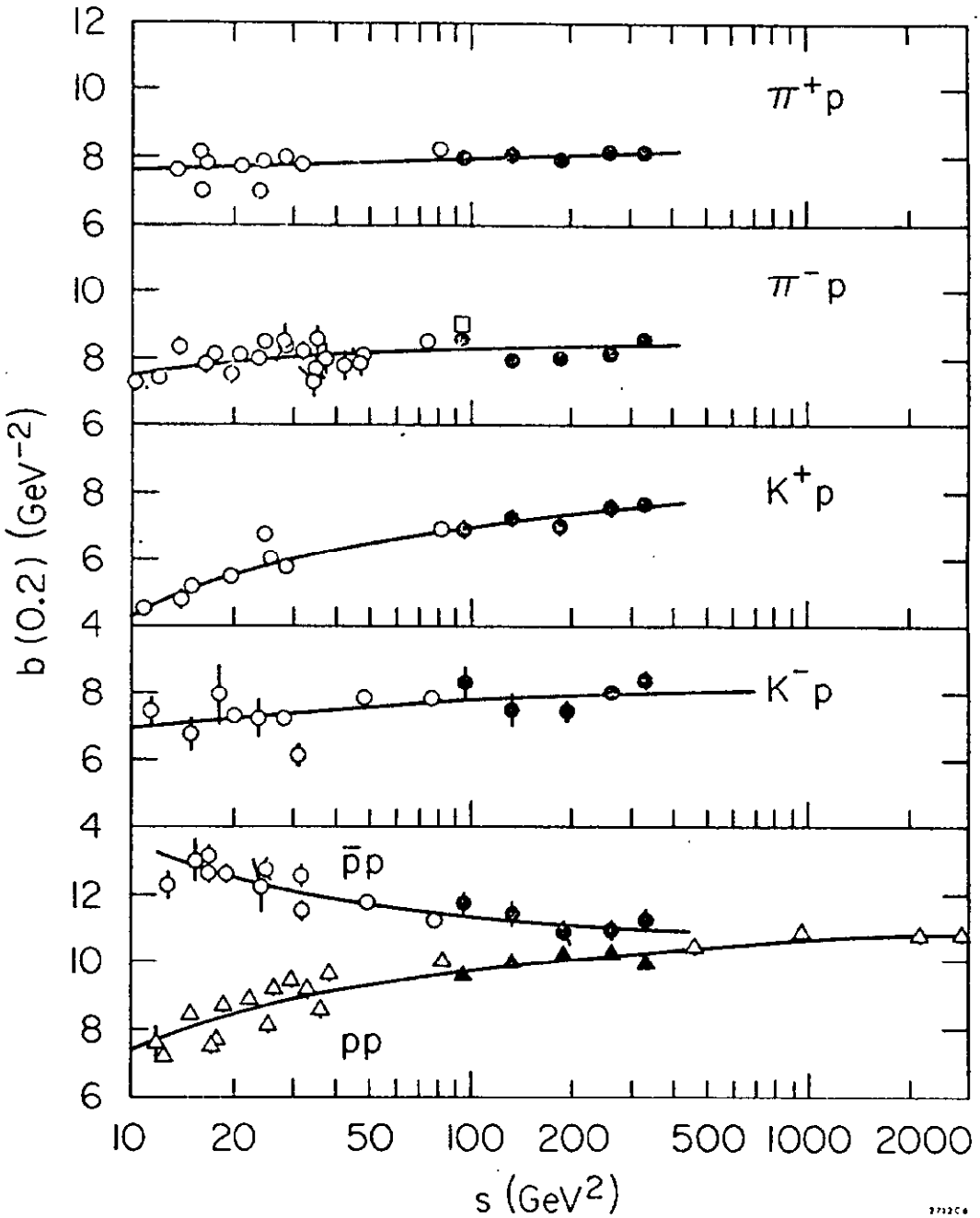
π^+p
π^-p
K^+p
K^-p
$\bar{p}p$
pp
b (0.2) (GeV^{-2})
s (GeV^2)
10
20
50
100
200
500
1000
2000

Figure 3